

Memory Effects in Nonequilibrium Transport for Deterministic Hamiltonian Systems

Jean-Pierre Eckmann,^{1,2} Carlos Mejía-Monasterio,¹ and Emmanuel Zabey¹

Received October 26, 2005; accepted June 8 2006

Published Online: July 12, 2006

We consider nonequilibrium transport in a simple chain of identical mechanical cells in which particles move around. In each cell, there is a rotating disc, with which these particles interact, and this is the only interaction in the model. It was shown in Ref. 1 that when the cells are weakly coupled, to a good approximation, the jump rates of particles and the energy-exchange rates from cell to cell follow linear profiles. Here, we refine that study by analyzing higher-order effects which are induced by the presence of external gradients for situations in which memory effects, typical of Hamiltonian dynamics, cannot be neglected. For the steady state we propose a set of balance equations for the particle number and energy in terms of the reflection probabilities of the cell and solve it phenomenologically. Using this approximate theory we explain how these asymmetries affect various aspects of heat and particle transport in systems of the general type described above and obtain in the infinite volume limit the deviation from the theory in Ref. 1 to first-order. We verify our assumptions with extensive numerical simulations.

KEY WORDS: heat transport

1. INTRODUCTION

In this paper, we study nonequilibrium transport in a class of 1-D Hamiltonian systems consisting of free noninteracting point particles of mass m moving inside a chain of identical cells, which are like “chaotic billiards.” Each cell contains a device (called a *tank* in Ref. 1) that interacts with the particles by exchanging energy with them. Even though the particles do not interact among themselves, an effective interaction is mediated by the tanks. As pointed out in previous studies,^(2,3) this mediated interaction among the particles allows such models

¹ Département de Physique Théorique, Université de Genève.

² Section de Mathématiques, Université de Genève.

to reach thermalization. These models are therefore genuine many-particle interacting Hamiltonian systems.⁽⁴⁾ Moreover, the details of the interaction between tanks and particles are not important. However, since our aim is to study model systems with realistic microscopic dynamics we shall ask that this interaction satisfies some general conditions: The system has to be time-reversible and Hamiltonian, although conservation of phase space volume is seemingly enough.

An earlier study,⁽¹⁾ went some ways in explaining the energy and particle profiles in terms of a stochastic approximation to a Hamiltonian model. This class of models was derived, in turn, from work^(2,3) in which a Lorentz gas with rotating discs was considered.

The stochastic approximation used in Ref. 1 assumed that in their evolution, the particles exit on both sides of each cell with *equal* probability at some fixed rate. Out of equilibrium, the exit rates will change from cell to cell and this leads to the effective transport of particles and heat. It was found that, to lowest order, due to the gradient character⁽⁵⁾ of the system, the profiles for the rates at which particles and energy are transported among neighboring cells interpolate *linearly* between the values imposed by the baths at the ends. From this, energy and particle density along the chain were computed explicitly. They are generally not linear.

The equal probability to jump to the left or to the right leads to a simple random walk process, without any memory effects. This assumption is strictly valid only when the cells are weakly coupled, *i.e.*, when the size of the openings connecting neighboring cells is very small. However, away from this limit case, the memory effects cannot in general be neglected and the symmetry assumption is likely to fail.

In this paper, we study the consequences of including these dynamical memory effects. The price we pay for doing this is the lack of a simple stochastic formulation to describe the energy exchange from cell to cell. Instead, at the steady state we propose a set of balance equations for the particle number and energy in each cell in terms of the reflection and transmission probabilities for particles and energy. We specify a phenomenological law for these probabilities that allows us to obtain an approximate expression for the steady state.

Our findings for the class of 1-D Hamiltonian chains that we consider can be summarized as follows:

1. We elaborate a phenomenological theory for the reflection and transmission probabilities for particles and energy.
2. Close to equilibrium, one can model the Hamiltonian system by persistent random walks. In this case the system remains of gradient type and thus, the theory of Ref. 1 is still applicable with corrections of the order of $1/N$ with N being the size of the system.
3. Far from equilibrium, we demonstrate that there is indeed a non-negligible dependence on the local gradients, and the corresponding profiles can be

shown to obey a non-linear differential equation that goes beyond linear response regime.

For our systems this asymmetry can be seen as a result of two different contributions: one which is purely geometrical and another which has a dynamical origin. For any scattering billiard (like the model cells) the reflection probability will in general be different from the transmission purely due to the geometry of the cell. When some source of interaction among the particles is considered, these coefficients will depend in addition on the local thermodynamical fields (namely, density and temperature) of the particles in the cell. When, in addition, the cell is subjected to an external thermodynamical gradient, the reflection and transmission probabilities will be different at the left and at the right of the cell. In this situation the dynamical asymmetry is emphasized.

Close to equilibrium, the geometric component dominates the dynamics, and then the asymmetry is *independent* of the local thermodynamical fields and thus, uniform along the chain. Furthermore, in this simpler case, the bias of the reflection/transmission coefficients is the *same* on both sides of any cell. The corresponding stochastic model is a persistent random walk process like that studied in Lorentz gases.⁽⁶⁾ After introducing the model in Sec. 2, 3 we sketch the stochastic approximation on which the results of the subsequent sections are inspired on. In Sec. 4, we study the case of constant asymmetry and show that one recovers the gradient property observed in Ref. 1, albeit with a slight correction in the slope of the jump rate profiles.

In the final sections, we analyze how the presence of *non uniform* local fields changes this picture. Clearly, since the tanks induce an interaction of the particles, the reflection (or transmission) probability depends on the local thermodynamical fields. We will distinguish two contributions to the dynamical asymmetry: one that depends on the mean values of the fields and another one that depends on the local gradients of the fields. These two effects are added to the purely geometrical contribution of the corresponding non-interacting system.

In order to judge the importance of the asymmetry phenomenon, we take fixed external fields and let the number of cells be sufficiently large. This is the standard limit taken in studies of the Fourier law.^(7,8) In our setting, the system is no longer of gradient type, and we obtain expressions for the transport equations which go beyond the standard linear regime. While these equations remain approximate, we verify numerically their validity even very far from equilibrium.

2. THE MECHANICAL MODEL

We consider a gas of noninteracting point particles of mass m that move freely inside a one-dimensional chain composed of N identical two-dimensional

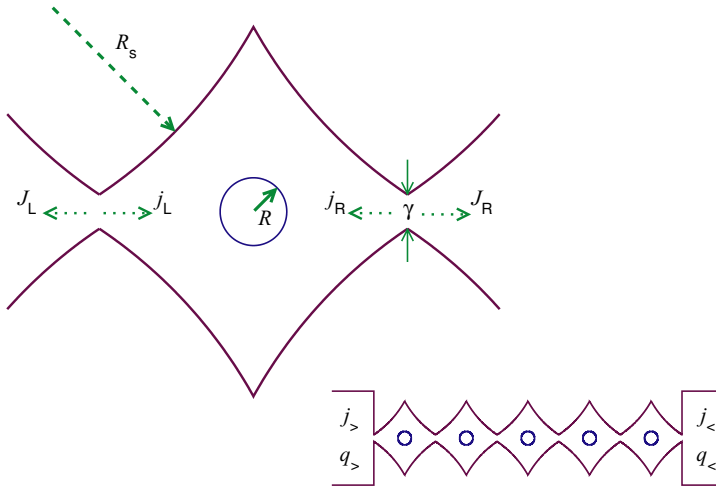


Fig. 1. Upper left: The geometry of a single cell for the rotating disc model. The boundary of the cell is made of four arcs of circles of radius R_s . The radius R of the rotating disc is chosen so that no trajectory can cross the cell without undergoing any collision. The arrows represent the incoming (j) and outgoing (J) rates of particles that cross the exits of width γ . The rates q and Q for the energy are not shown. Lower right: A chain of 5 cells connected to two baths. (Color online).

cells, arranged horizontally. Each cell is connected to its left and right neighbors through two openings of size γ .

Inside each cell there is a mechanical “tank” capable of storing a certain amount of energy. When a particle hits the tank, some energy exchange takes place, and this is the only interaction in the model.

While the details of this interaction are largely irrelevant for the discussion in this paper, our simulations have been done for the following precise setup which we call the rotating disc model (RDM). Each cell has the geometry described in Fig. 1. The energy tank is modeled by a freely rotating disc which is pinned at the center of the cell. Its energy is only rotational. When a particle hits the disc, it exchanges its tangential velocity v_t with the angular velocity ω of the disc, while the normal component v_n is reflected⁽²⁾:

$$\omega' = v_t, \quad v_t' = \omega, \quad v_n' = -v_n. \quad (2.1)$$

Note that while the particles do not see each other, they effectively interact through their collisions with the tanks. Thus local equilibrium can be reached.⁽⁹⁾ The model is by no means free.

The chain is connected at both ends to two reservoirs of particles through openings of the same size γ . The reservoirs are idealized as infinite chambers

containing an ideal gas at a certain density n and temperature T . When we study non-equilibrium effects, n and T will differ at both ends.

Another variant of this model has the same fixed walls, but the disc is replaced by a rotating needle, with elastic collision, conserving total energy (and total angular momentum).

These models are among a class of models satisfying the following minimal assumptions:

- *Time reversibility*: The trajectory of the system in phase space across a scattering event must be time reversible. While this condition is not really necessary for our derivations, our aim is to model realistic macroscopic situations for which microscopic time-reversibility is believed to hold.
- *Conservation of phase-space volume*: This condition is not as strong as requiring the dynamics to be Hamiltonian, and seems to lead to similar results. In particular, the rotating disc model satisfies this condition but is not Hamiltonian: Its collision rule preserves phase space volume but is not a canonical transformation.

We call the models satisfying these two assumptions **mechanical**.

We end the description of the model by a more detailed account of the heat and particle baths. From the left reservoir at density $n_>$ and temperature $T_>$, particles are injected into the system at a rate $j_>$. Observe that the mean energy of the particles injected into the system is not $T_>$ but $\frac{3}{2}T_>$ (see *e.g.*, Ref. 1). Thus, the left reservoir injects energy into the system at a rate $q_>$ given by

$$q_> = \frac{3}{2} j_> T_>.$$

Analogously, the right reservoir injects particles and energy at rates $j_<$ and $q_<$ respectively. Each injected particle will be eventually re-absorbed by one of the reservoirs and this happens when it crosses into that reservoir. All information about that particle is then discarded.

As the reservoirs consist of an ideal gas, the injection rate j is a function of the density n and temperature of the reservoir given by

$$j \propto \gamma n T^{1/2}. \tag{2.2}$$

Furthermore, the chemical potential at the reservoirs can be written in terms of the injection rate as

$$\mu = T \log \left(\frac{\lambda_0 j}{T^{3/2}} \right) \tag{2.3}$$

with λ_0 some constant.

We end the section with some comments on the choice of the model: Our choice of the reflecting boundaries of Fig. 1 is to guarantee the desirable ergodic

and mixing properties of chaotic billiards. However, we have not succeeded in showing rigorously that the cell is either ergodic or mixing. While the geometry of the rotating needles model (RNM) is similar to that of the RDM, there are two main differences: First, the RNM is not only mechanical but Hamiltonian. Second, in the RNM model, a particle can in principle cross many cells without hitting any needles or boundaries. This may produce logarithmic corrections to transport, which are beyond our study.

3. AN APPROXIMATE STOCHASTIC MODEL

In Ref. 1, a stochastic approximation of the mechanical model was considered. In this approximation it was assumed that what happens in one cell is independent of the state of the other cells. The particles perform a random walk among the cells, mixing their energies with the tanks according to rules which mimic the mechanical system described above. Once the particle has mixed its energy, it waits (until an exponential clock rings) and then jumps with equal probability to the left or to the right. With these assumptions it was found that the rates at which particles and energy jump among neighboring cells are linear functions of the position and from this, energy and particle density along the chain can be computed explicitly under very general assumptions. However, note that these assumptions are valid when the cells are weakly coupled and dynamical memory effects appear when this is not the case.

The purpose of this paper is to study the consequences of these memory effects on the transport properties of the mechanical models that we consider here. The price we pay is that the stochastic model, used in Ref. 1 is not longer appropriate. We briefly sketch the essentials of this stochastic approximation that will serve us as a guideline to our analysis (we refer the interested reader to Ref. 1 for more details about this).

The stochastic description is based on particles, carrying energies, and the discs (as in Ref. 1). Each state of the cell is represented by a point in $\Omega = \cup_m \Omega^m$ where $\Omega_m = \{(x_1, \dots, x_m), (p_1, \dots, p_m), y\}$ and m is the number of particles in the cell at some given time, x_i are their energies, $p_i \in \{-1, 1\}$ specifies the side on which the particle enter the cell and y is the energy stored by the disc. For a chain with N cells, the phase space is $\Omega^{(N)} = \Omega \times \Omega \times \dots \times \Omega$ with N factors. The reservoirs at the ends absorb particles, and eject them at a rate $j_>$ resp. $j_<$ (for left and right) and with an exponential distribution of energy (with mean temperatures $T_>$ and $T_<$).

The stochastic process is as follows (see Ref. 1 for more details): When a particle entered a cell k from the left, it will wait for an exponentially distributed time (whose mean may depend on its energy), it mixes energy with the disc, and leaves the cell (after another exponential waiting time) with probability $\alpha_{L,k}^J$ to the left, and with probability $1 - \alpha_{L,k}^J$ to the right.

This stochastic description leads, in the steady state, to the balance equations for rates of particle injection (see (3.1) below).

However, while this description is adequate for particle flux, it is too detailed for the energy flux. Instead of trying to formulate a stochastic process for both particle and energy fluxes (see Ref. 11 for an example), we elaborate a phenomenological theory for the physical parameters involved. We show that this information is enough to obtain precise results on the average properties of the steady state of this type of systems.

It is convenient to distinguish the local *incoming* rates from the *outgoing* rates. We denote by $J_{L,k}$ and $Q_{L,k}$ the rates at which particles and energy exit the k -th cell to the left and by $J_{R,k}$, $Q_{R,k}$ those to the right. The exit rates are then simply determined by the corresponding incoming rates $j_{L/R,k}$ and $q_{L/R,k}$, and by reflection $\alpha_{L,k}$, $\alpha_{R,k}$ coefficients which will satisfy the balance equations (for the cell k):

$$\begin{aligned}
 J_{L,k} &= \alpha_{L,k}^J j_{L,k} + (1 - \alpha_{R,k}^J) j_{R,k}, \\
 J_{R,k} &= (1 - \alpha_{L,k}^J) j_{L,k} + \alpha_{R,k}^J j_{R,k}, \\
 Q_{L,k} &= \alpha_{L,k}^Q q_{L,k} + (1 - \alpha_{R,k}^Q) q_{R,k}, \\
 Q_{R,k} &= (1 - \alpha_{L,k}^Q) q_{L,k} + \alpha_{R,k}^Q q_{R,k}.
 \end{aligned}
 \tag{3.1}$$

Note that even for (left-right) symmetric cells, out of equilibrium the reflection coefficients at the left and right of the cell are not necessarily equal. The balance equations account for the conservation of energy and particle number, namely $Q_{L,k} + Q_{R,k} = q_{L,k} + q_{R,k}$ and $J_{L,k} + J_{R,k} = j_{L,k} + j_{R,k}$. Since an average the steady state is assumed, mean rates appear in (3.1).

We define the coefficients by empirical probabilities $j_{LR} \dots$ by (omitting the index k for better legibility)

$$\begin{aligned}
 \alpha_L^J &= \frac{j_{LL}}{j_L}, \quad \alpha_R^J = \frac{j_{RR}}{j_R}, \\
 \alpha_L^Q &= \frac{1}{2} + \frac{q_{LL} - q_{LR}}{2q_L}, \quad \alpha_R^Q = \frac{1}{2} + \frac{q_{RR} - q_{RL}}{2q_R},
 \end{aligned}
 \tag{3.2}$$

where, for example, j_{LR} is the rate of particles leaving on the right, which entered on the left, and q_{LR} is the mean energy carried out by particles which entered on the left. If we denote $p(E'|E)$ the conditional probability that a particle entering with energy E leaves with energy E' and by $\alpha_{LL}(E', E)$ the probability that it leaves on the left when it entered on the left, then one can think of q_{LL} as

$$q_{LL} = \int dE' dE E' \alpha_{LL}(E', E) p(E'|E),$$

where the complicated dependence on the state of the system is neglected (that is, we do not consider the density and the other particles in this formula). Instead we will use a phenomenological description for the reflection coefficients. Perhaps it is useful to note that with the above conventions,

$$j_{LL} = \int dE' dE \alpha_{LL}(E', E) p(E'|E).$$

The definition for the α^J is canonical, but for the α^Q we chose a more complicated expression: It simultaneously preserves total energy conservation, but allows for an energy change during scattering. The reader should note that the quantities α , J , Q are mean values averaged on the (fluctuating) steady state. An important aspect of the present work is to check that this approximation still captures the essentials of transport of heat and particles.

To further simplify the discussion, we make the approximate assumption that the α_Y^X (for all $X \in \{J, Q\}$ and $Y \in \{L, R\}$) only depend on the incoming fluxes. Due to the mechanical nature of the models considered here, the time scale is a free variable leading to the scaling relation

$$\alpha(j_L, j_R, q_L, q_R) = \alpha(\lambda j_L, \lambda j_R, \lambda^3 q_L, \lambda^3 q_R), \quad (3.3)$$

for all $\lambda > 0$. Therefore, α only depends on 3 ratios. It will be useful to distinguish the contribution to α that arises out of equilibrium from the contribution that only depends on the mean values of the fields. Accordingly we write

$$\alpha(j_L, j_R, q_L, q_R) = \alpha_G \left(\frac{j^{3/2}}{q^{1/2}} \right) + \varepsilon \left(\frac{j^{3/2}}{q^{1/2}}, \frac{j_R - j_L}{j_R + j_L}, \frac{q_R - q_L}{q_R + q_L} \right), \quad (3.4)$$

and require that $\varepsilon(j^{3/2}/q^{1/2}, 0, 0) = 0$, *i.e.*, that ε vanishes at equilibrium. The term α_G , which has a purely geometric origin, describes in turns those aspects which hold at thermal equilibrium and the term $j^{3/2}/q^{1/2}$, with $q = (q_L + q_R)/2$ and $j = (j_L + j_R)/2$, is proportional to the density (see Eq. (2.2)).

Note that $\alpha_Y^X = \frac{1}{2}$ corresponds to the simple symmetric random walk considered in Ref. 1. The case when the α_Y^X are independent of the local fields, but different from $\frac{1}{2}$ corresponds to a persistent random walk and will be studied in the next section. More general and realistic laws will be investigated in the last sections.

Also note that the details of the dynamics, in particular those that depend on the specific model, are encoded by Eq. (3.4). To show the validity of our approach we will proceed as follows: We first introduce the law (3.4). This closes the balance equations for the energy and particle number. We next determine the thermodynamical profiles and currents. Finally we compare these “theoretical” profiles to those obtained with numerical simulations of the mechanical model.

4. SOLUTION OF THE STOCHASTIC MODEL NEAR EQUILIBRIUM

In this section, we discuss profiles in the infinite volume limit with fixed boundary conditions, under the approximating assumption that every cell is at local equilibrium. This means that we neglect the term ε in Eq. (3.4) and thus, $\alpha_{R,k}^J = \alpha_{L,k}^J = \alpha_G^J$ and similarly for the α^Q . Furthermore, we make the assumption, that α_G^J and α_G^Q are independent of the densities found in the chain. In this approximation the reflection coefficient is a constant independent of the thermodynamical fields and thus, independent of position. The exact range of validity of this assumption will be discussed in Sec. 5. Our approximations mean that we are dealing with the case of a persistent random walk, and the current section, while “well-known” in principle, serves as a first check of the validity of our approximations. Once this check has been done, we will study in more detail the corrections to the persistent case.

Since the geometric contribution is the only one remaining in (3.4), we refer to this case as the *geometric approximation*. Note that this contribution will lead in general to a reflection coefficient different from $\frac{1}{2}$. This approximation corresponds to a persistent random walk in which the probability for the walker to move forward is different from the probability to move backwards.

We discuss the total ejection rates $J_k = J_{L,k} + J_{R,k}$ and $Q_k = Q_{L,k} + Q_{R,k}$. The boundary conditions of the problem are simply

$$j_{>} = j_{L,1}, \quad j_{<} = j_{R,N}, \quad q_{>} = q_{L,1}, \quad q_{<} = q_{R,N}. \quad (4.1)$$

From now on we will use rescaled variables $\xi = k/(N+1) \in [0, 1]$, and let $J(\xi) = J_k$ and $Q(\xi) = Q_k$. For the sake of simplicity, we will only write α^J and α^Q .

Lemma 4.1. *Under the assumptions made above, the particle and energy ejection rates satisfy*

$$J(\xi) = 2(j_{>} + \xi \times \Delta j) + \frac{(1 - 2\alpha^J)(1 - 2\xi)}{1 + (N-1)\alpha^J} \Delta j, \quad (4.2)$$

where $\Delta j = j_{<} - j_{>}$, and

$$Q(\xi) = 2(q_{>} + \xi \times \Delta q) + \frac{(1 - 2\alpha^Q)(1 - 2\xi)}{1 + (N-1)\alpha^Q} \Delta q, \quad (4.3)$$

with $\Delta q = q_{<} - q_{>}$.

Remarks: The first term in the *r.h.s.* of Eqs. (4.2) and (4.3) corresponds to the result obtained in Ref. 1. The last terms account for the correction when $\alpha \neq \frac{1}{2}$. These corrections disappear in the infinite volume limit. The integral over ξ of the correction vanishes, because of energy and particle conservation. Also, note that

as α is a constant, the profiles are linear (even when $\alpha \neq \frac{1}{2}$), because the system is still of gradient type.

Proof: The proof is just a calculation. We will concentrate on the case of particle rates. This calculation starts from (3.1). Using the identities Eq. (4.1), we can solve (3.1) for the remaining J and obtain for $k = 1, \dots, N$,

$$\begin{aligned} J_{L,k} &= \frac{(N-k+1)\alpha}{1+(N-1)\alpha} j_{>} + \frac{1+(k-2)\alpha}{1+(N-1)\alpha} j_{<}, \\ J_{R,k} &= \frac{1+(N-k-1)\alpha}{1+(N-1)\alpha} j_{>} + \frac{k\alpha}{1+(N-1)\alpha} j_{<}. \end{aligned} \quad (4.4)$$

Then, summing the R and L terms, we get

$$J_k = \frac{1+2(N-k)\alpha}{1+(N-1)\alpha} j_{>} + \frac{1+2(k-1)\alpha}{1+(N-1)\alpha} j_{<}. \quad (4.5)$$

Rearranging terms one immediately obtains (4.2). The case (4.3) is handled similarly.

Therefore, if the value for α is known, the profile of the ejection rates can be obtained from the solution (4.4) for any nonequilibrium state, as long as α is independent of the external parameters. \square

4.1. Thermodynamical Profiles

In order to identify temperature and particle density, we use the techniques of Ref. 1. In that paper, it was observed that in equilibrium, a single cell has a Poisson distribution of particle number with mean n and a canonical distribution of the total energy in the cell (particles and disc) with a temperature T . Furthermore, (see Proposition 4.1 in Ref. 1) one has universal relations between these quantities and the properties of the reservoir, namely

$$\begin{aligned} T &= \frac{2}{3} \frac{Q}{J}; \\ n &= \eta_0 \frac{J^{3/2}}{Q^{1/2}}. \end{aligned}$$

The constant η_0 depends only on the geometry of the cell and the size of the opening, but not on the shape

$$\eta_0 = \sqrt{\frac{3\pi}{4}} \frac{\text{Area}(\Gamma)}{|\gamma|}, \quad (4.6)$$

where the area is that of the cell minus the disc and where $|\gamma|$ is the size of the opening between adjacent cells. This identification is unique provided the system is ergodic.³

Assuming local equilibrium at any cell k in the system, the formulas above generalize immediately to predictions of the profiles for temperature and particle number (with $\xi = k/(N + 1)$)

$$T(\xi) = \frac{2}{3} \frac{Q(\xi)}{J(\xi)}; \tag{4.7}$$

$$n(\xi) = \eta_0 \frac{J^{3/2}(\xi)}{Q^{1/2}(\xi)}. \tag{4.8}$$

Note that while the jump rates Q and J have linear profiles in the current approximation the profiles of T and n are generally nonlinear. In Sect. 6 we will study in detail the deviations from linearity of Q and J .

To test these results we performed out of (but close to) equilibrium simulations for a chain of 20 RDM cells with $|\gamma| = 0.08$, $R_s = 1.15$ and a disc radius of $R = 0.0793$ (ensuring that no particle can cross a cell without being scattered). The choice parameters used in the simulations are a compromise between good mixing within each cell, and the speed of convergence to the stationary state.

We checked in our simulations for the Hamiltonian model that the profiles of the outgoing rates are described by (4.2) and (4.3). In Fig. 2 we show the temperature and density profiles for two different simulations, in which the baths were set to $j_> = 10$, $j_< = 12$, $T_> = 1000$ and $T_< = 1100$ (circles), and $j_> = 12$, $j_< = 10$, $T_> = 1000$ and $T_< = 1300$ (triangles).

To compare the measured profiles for T and n with our analytical expressions we have first numerically computed the reflection coefficients α^J and α^Q for each cell. For both simulations we found that both coefficients are constant (to within numerical accuracy) along the chain with a mean value of $\alpha^J = 0.5585 \pm 10^{-4}$ and $\alpha^Q = 0.5609 \pm 10^{-4}$. We insert these values into (4.2)–(4.3) and obtain estimates for the profiles of the outgoing rates $J(\xi)$ and $Q(\xi)$. We then use these estimates in (4.7) and (4.8) to obtain the profiles for the energy T and the number of particles n , as predicted by our theory. These are shown as solid lines in Fig. 2. The fit with the directly measured profiles for T and n is excellent. Note that these profiles are not expected to be linear.⁽¹⁾ This non-linearity has already been verified against the theory in Ref. 1, but here we study rather the effect of the asymmetry. At this order of approximation, that is, in the case of the persistent α 's the difference between the two approaches is only of order $1/N$ and is not yet visible in the simulations.

³The definition of η_0 differs from that of Ref. 1 because of different normalizations of the kinetic energy.

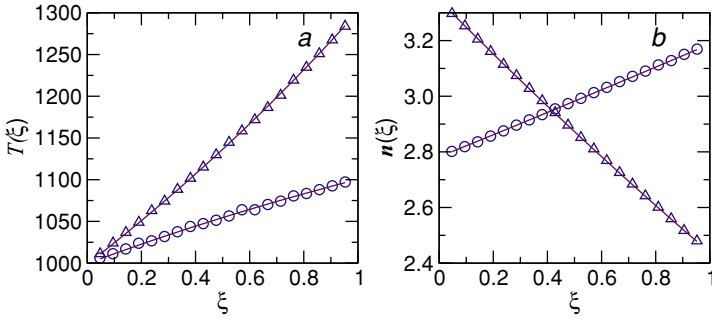


Fig. 2. Comparison of the measured profiles with those predicted by the Eqs. (4.7) and (4.8), using (4.2)-(4.3). The measured profiles were obtained as an average over 400 different realizations of the RDM for 20 cells. The energy profile $T(\xi)$ (a) and the particle density profile $n(\xi)$ (b) are shown for two different simulations with $j_> = 10, j_< = 12, T_> = 1000$ and $T_< = 1100$ (circles) and $j_> = 12, j_< = 10, T_> = 1000$ and $T_< = 1300$ (triangles). For all data the error bars are smaller than the symbol size. The solid lines in each panel correspond to the analytical profiles of Eqs. (4.7) and (4.8) for $\alpha^J = 0.5585$ and $\alpha^Q = 0.5609$ as explained in the text. (Color online).

4.2. Macroscopic Currents

The heat and matter local macroscopic currents can be easily derived from the balance equations. The current of particles between the k -th and $k + 1$ -st cells is defined as $\varphi^J = J_{R,k} - j_{R,k}$ or, in terms of outgoing jump rates as $\varphi^J = J_{R,k} - J_{L,k+1}$. Using Eq. (4.4) we obtain

$$\varphi^J = -\frac{1 - \alpha^J}{1 + (N - 1)\alpha^J} \Delta j, \quad (4.9)$$

where the result is of course independent of k . In an analogous way, $\varphi^Q = Q_{R,k} - Q_{L,k+1}$, and we obtain for the heat current

$$\varphi^Q = -\frac{1 - \alpha^Q}{1 + (N - 1)\alpha^Q} \Delta q. \quad (4.10)$$

In these variables, the currents are linear functions of the external gradients.

In the numerical simulations described above, we also computed the heat and matter currents obtaining an average value of: $\varphi^J = -0.077 \pm 0.002$ and $\varphi^Q = -185 \pm 13$ (for the experiment in circles in Fig. 2) and $\varphi^J = 0.08 \pm 0.008$ and $\varphi^Q = -56 \pm 4$ (for the experiment in triangles of the same figure). If instead we insert the numerically computed values for α^J and α^Q into Eqs. (4.9) and (4.10) we obtain $\varphi^J = -0.076$, $\varphi^Q = -180.8$ (circles) and $\varphi^J = 0.076$, $\varphi^Q = -56.5$ in perfect agreement with the numerical experiment to within numerical accuracy.

Therefore, we conclude that in cases in which the α probability can be taken to be constant along the chain, the conclusions of Lemma 4.1 describe remarkably

well the transport properties of the disc model. Similar results were found for the needle model, and we conjecture that this extends to many similar models.

The validity of the linear transport Eqs. (4.9) and (4.10) depends crucially on the property that $\alpha_L = \alpha_R$. For high gradients, this property is violated as we show in Sec. 6. In that case, the Fourier law does not hold, but the flux still scales as $1/N$ for large systems. The reason is that local gradients appear in the diffusion constants.

We remark finally that α (and thus the details of the cell) determines the nature of the macroscopic transport: If $\alpha = 0$ the transport along the chain is ballistic as the currents do not scale with the size of the system N . On the other hand, if $\alpha = 1$ the chain behaves as an insulator. For any other value of α the transport is normal with well defined transport coefficients.

5. VALIDITY OF THE GEOMETRIC APPROXIMATION

In the previous section, we assumed that the reflection coefficient α , while not necessarily equal to $\frac{1}{2}$, neither depends on the particle density inside a cell nor on the strain acting on it. In other words, $\alpha_{R,k}^J = \alpha_{L,k}^J = \alpha_G^J$, this value being determined by the geometry of the cell only (and similarly for α^Q).

In this section we discuss this assumption and determine the range of parameters for which it applies with high precision. The discussion will also clarify the choice of the decomposition (3.4). The profiles obtained when α_R and α_L are different and vary along the chain are discussed in the next section.

The reader should first note a simple fact: When the discs (tanks) in the cells are not allowed to rotate, and the reflection is specular, then the trajectories are independent of the energy and of the particle density. In that case α is clearly independent of all external parameters (and $\alpha^J = \alpha^Q$ since the particles are the only energy carriers). Therefore, any variation of α has its origin in the effective interaction of the particles.

The interaction changes the dynamics inside the cell, but does not always induce a variation of α . We first consider an ideal case: particles are always trapped in the cell for a very long time. They collide with the tank many times, and forget the side from which they entered the cell, as well as the energy they had at that time. In this case, the thermalization of the particles is perfect *due to the interaction* and no asymmetry appears.

The geometric approximation loses its validity due to two related memory effects:

- The distribution of energy in the cell is not uniform, and thus thermalization is only approximate
- Particles retain a memory of the energy they had when entering the cell, and this effect is energy-dependent.

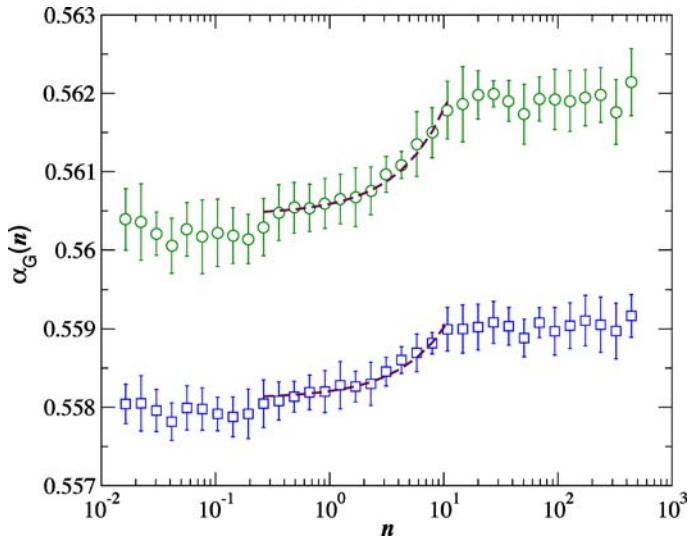


Fig. 3. Dependence of the equilibrium reflection probabilities α_G^J (squares) and α_G^Q (circles) on the density of particles in the cell n for the RDM with $\gamma = 0.08$. Note that α_G saturates to a constant value at low and high densities. At intermediate densities $0.3 < n < 10$, α_G grows linearly with density as corroborated by the linear fits (dashed lines). The fits are $\alpha_G^Q(n) = 0.56048 \pm 2 \cdot 10^{-5} + (1.29 \cdot 10^{-4} \pm 5 \cdot 10^{-6})n$, and $\alpha_G^J(n) = 0.55813 \pm 2 \cdot 10^{-5} + (8.71 \cdot 10^{-5} \pm 5 \cdot 10^{-6})n$. (Color online).

In order to test these properties, we first performed *equilibrium* simulations. These will isolate the geometric contributions to the α 's. This allows us, in the next section, to identify those contributions which are typical of non-equilibrium, justifying thereby the decomposition of Eq. (3.4). In Fig. 3 we show the dependence of the reflection probabilities α_G^J and α_G^Q on the density of particles n for a single cell (for the RDM). Injection rates of the reservoirs are chosen according to (2.2) in order to obtain the desired densities. We observe the following:

- For low densities ($n \lesssim 0.3$) and high densities ($n \gtrsim 10$), the α is practically constant. Therefore, if a whole chain of cells is in either of these regimes, we can model it with a constant α . If in addition, the local gradients are small, then the system is (close to) gradient type, and is well described by the approximations of Sec. 4.
- For intermediate densities, α increases linearly with the density. This is a new kind of regime (not of gradient type), which we discuss in more detail in the next section.

As discussed in Sec. 3, the distinction in Eq. (3.4) between the geometric contribution α_G and the dynamical ε , is that while ε depends on the local gradients of the thermodynamical field (and is zero at equilibrium), α_G will depend at

most on the mean fields. Therefore, we can expect that a constant reflection coefficient will always remain a good approximation close to equilibrium, namely when $\Delta T/T \ll 1$ and $\Delta n/n \ll 1$. In that case, the equations of the Sec. 4 hold, regardless of the average density of the system.

The reader should observe that α_G^Q and α_G^J differ, while for a system without memory effect (such as the Lorentz model) one would expect equality of these quantities. This difference is not an artifact of our simulations but a property of mechanical models of the type we consider. Looking at Fig. 1, and the collision rule (2.1), the reader will realize that fast particles have a higher probability to exit after only 1 collision with the disc than slower ones, because the angle of reflection tends to be smaller for the fast ones. Therefore the memory effect depends on the individual energies and not the mean, and this accounts for the difference above. We have checked that by placing non-rotating discs between the openings and the turning disc, the effect is reduced.

We now turn our attention to *nonequilibrium* effects, which are described by the functions ε_Y^X of Eq. (3.4). We performed simulations for the single cell RDM in which the external gradients were kept fixed but the mean temperature was changed ($T_> = T - \Delta T/2$ and $T_< = T + \Delta T/2$). In the inset of Fig. 4, we show the left and right reflection coefficients, α_L^J and α_R^J , as a function of $\Delta T/T$. As the parameters approach equilibrium values, the difference $|\alpha_L^J - \alpha_R^J|$ is seen to decay to zero (at a rate $(\Delta T/T)^{5/2}$). The value that α_L^J and α_R^J take in equilibrium is the constant geometric asymmetry (which for these parameters are $\alpha_G^J \sim 0.558$ and $\alpha_G^Q \sim 0.560$). At the other extreme, since the temperature cannot be negative, $\Delta T/T \leq 2$. The difference $\Delta\alpha$ is maximal at $\Delta T/T = 2$. Interestingly, $\alpha_L^J(\Delta T/T = 2)$ corresponds to the reflection coefficient of the Lorentz gas, *i.e.*, to the limit in which the central disc does not rotate.

6. FAR FROM EQUILIBRIUM

In Sec. 4 we have assumed that the system is at local equilibrium, and that the particle density varies in a range where the α_G are essentially constant. In this section, we discuss the case when both these assumptions are dropped. This means that we take into account the dependence of the α on the density and on the local gradients of the thermodynamical fields.

Far from equilibrium, the distribution of the local fields will be different from cell to cell and thus, the probabilities will depend on the position along the chain $\alpha \equiv \alpha(\xi)$. We recall the set of equations Eq. (3.4) for α one of the functions α_Y^X :

$$\alpha(j_L, j_R, q_L, q_R) = \alpha_G \left(\frac{j^{3/2}}{q^{1/2}} \right) + \varepsilon \left(\frac{j^{3/2}}{q^{1/2}}, \frac{j_R - j_L}{j_R + j_L}, \frac{q_R - q_L}{q_R + q_L} \right).$$

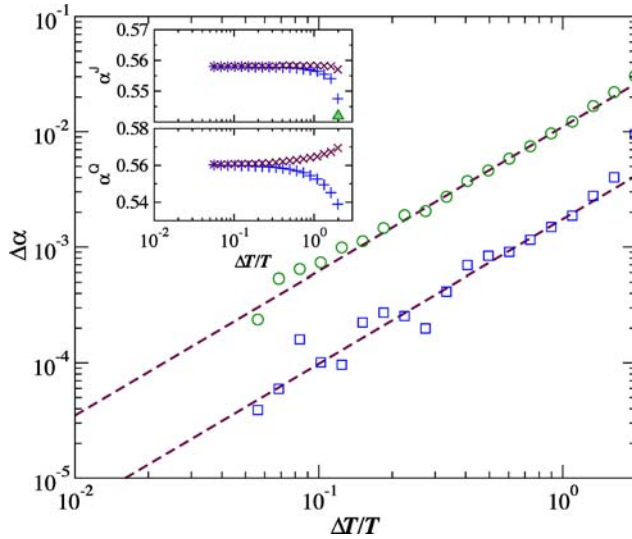


Fig. 4. Difference $\Delta\alpha = \alpha_R - \alpha_L$ as a function of $\Delta T/T$ for α^J (squares) and α^Q (circles). Each symbol corresponds to a simulation for the single cell RDM with a geometry as in Fig. 2 but $|\gamma| = 0.08$. In all experiments the external gradients were fixed to $j_> = j_< = 1$, $\Delta T = T_< - T_> = 100$ and $\frac{1}{2}(T_> + T_<) = T$. The dashed lines correspond to $\Delta\alpha \sim (\Delta T/T)^{5/2}$. In the inset α^J and α^Q at the left (plus) and right (crosses) boundaries are shown. Note that $\Delta\alpha \rightarrow 0$ on approach to equilibrium, while for very large gradients α_L^J reaches the Lorentz gas limit indicated by the hashed triangle (see the text for a discussion). (Color online).

It is understood that α_G and ε denote functions which are different for the various α_Y^X , but have the following common properties: By definition, ε must vanish at equilibrium

$$\varepsilon_Y^X(x, 0, 0) = 0.$$

Furthermore, the left-right symmetry of the cell implies:

$$\varepsilon_L^X(x, y, z) = \varepsilon_R^X(x, -y, -z). \tag{6.1}$$

We next discuss specific properties of ε as they appear from numerical simulations for the RDM. It turns out that the ε_Y^X not only vanish on the submanifold $(x, 0, 0)$, but, to a very good approximation they vanish for those points where the temperatures T_L and T_R are equal. Since the temperatures are functions of the injection rates of particles and energy this means that ε_Y^X vanishes on the submanifold of $\{j_L, j_R, q_L, q_R\}$ where $T_L = T_R$. While we have no proof of this observation, it can be understood by observing that for $T_L = T_R$ the tank has the same temperature as all the particles, and therefore we are in presence of purely geometric phenomena which are already captured by the function α_G alone.

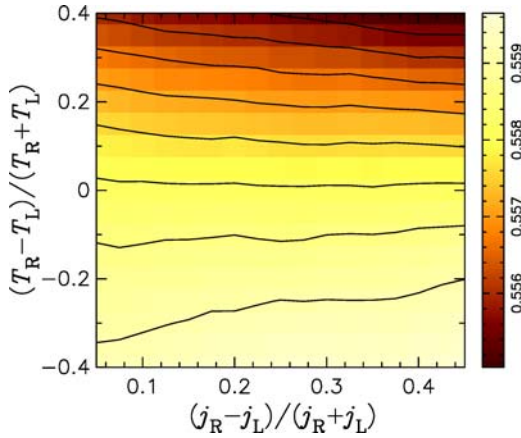


Fig. 5. Contour density plot of α_L^J as a function of the local gradients in j and T . The obtained values correspond to the one-cell RDM with an opening of $\gamma = 0.08$. Note that the contour line for $T_L = T_R$ is horizontal, justifying Eq. (6.2). (Color online).

We expand ε_Y^X to first order, and in view of the above information, a very good approximation is given by assuming that ε has the form:

$$\varepsilon = \varepsilon_0 \frac{T_R - T_L}{T_R + T_L} + \varepsilon_1 \frac{T_R - T_L}{T_R + T_L} \times \frac{j_R - j_L}{j_R + j_L}, \tag{6.2}$$

where ε_0 and ε_1 are constants depending on the choice X, Y .

We have numerically corroborated Eq. (6.2) for the RDM. In Fig. 5 a contour density plot for α_L^J is shown as a function of the local gradients. The linearity of the contours shows that α_L^J is a linear function of the local gradient in j whose slope and intercept depends on the local gradient of temperature. The same behavior is found for the other coefficients.

The reader should note that for fixed external parameters (for the heat and particle reservoirs) and for long chains, the local gradients per cell scale like $1/N$ and thus, one expects the ε to be both proportional to $1/N$ and to the force fields. The question then is whether the effect of the asymmetry will disappear in the infinite volume limit or not.

We next show how, in principle, the above approximations lead to a closed system of equations for the profiles, and we then check, for one particular case that the equations indeed describe the profiles found in numerical experiments, and account correctly for the deviation from Ref. 1.

Since the local gradients are naturally expressed in terms of the injection rates we use the identification between injection and ejection rates to write Eq. (3.1) as

$$j_{R,k-1} = \alpha_{L,k}^J j_{L,k} + (1 - \alpha_{R,k}^J) j_{R,k},$$

$$j_{L,k+1} = (1 - \alpha_{L,k}^J) j_{L,k} + \alpha_{R,k}^J j_{R,k}, \tag{6.3}$$

with $k = 1, \dots, N$ and boundary conditions $j_{L,1} = j_{>}$ and $j_{R,N} = j_{<}$.

Using the definition of the particle current $\varphi^J = j_{L,k+1} - j_{R,k}$, one can eliminate the j_R (or the j_L), and the Eqs. (6.3) in which case the system reduces to only one equation:

$$(1 - \alpha_{L,k}^J) j_{L,k} - (1 - \alpha_{R,k}^J) j_{L,k+1} + \alpha_{R,k}^J \varphi^J = 0. \tag{6.4}$$

Analogous expressions are obtained for the energy injection rates.

It is here that the non-gradient nature of our models is visible in a nutshell. For (6.4) to be of gradient type one needs to have $\alpha_{L,k}^J = \alpha_{R,k}^J$. As we have seen in Fig. 4, this is, in general, not the case.

6.1. Infinite Volume Limit

We take the continuum limit of Eq. (6.4), with cells of size $1/N$ so that the rescaled variable $\xi = k/(N + 1)$ is in the domain $[0, 1]$. Note that the currents φ^J and φ^Q scale (for fixed external forces) like $1/N$.

In order to close the balance equation for j_L one substitutes the ansatz (6.2) into Eq. (6.4). This leads to an involved, but in principle straightforward system of nonlinear differential equations, which we do not write down. However, we will deal with the special simpler case in which $q(\xi)$ is approximately constant along the chain.

When q is constant, one finds that $T \propto 1/j$ and therefore the assumption (6.2) can be reformulated for the corresponding ε_L and ε_R to first order in $1/N$ as

$$\varepsilon_{L,k}^J = \mathcal{A}^J \frac{j_{R,k} - j_{L,k}}{j_{R,k} + j_{L,k}}, \quad \varepsilon_{R,k}^J = -\mathcal{A}^J \frac{j_{R,k} - j_{L,k}}{j_{R,k} + j_{L,k}}, \tag{6.5}$$

where $\mathcal{A}^J = -\varepsilon_0$ are constants determined by the boundary conditions of (6.4). The minus sign in the equation for $\varepsilon_{R,k}$ is a direct consequence of (6.1).

We have numerically corroborated the hypothesis (6.5). In Fig. 6 we show the dependence of the asymmetries ε^J and ε^Q on the gradients of the local injection rates for a chain of 20 RDM cells. The asymmetries are seen to depend linearly on the local gradient of j . Farther from equilibrium (not shown), deviations will appear.

Using the particle current we express the asymmetry (6.5) in terms of the j_L alone as

$$\begin{aligned} \varepsilon_{L,k}^J &= \mathcal{A}^J \frac{j_{L,k+1} - j_{L,k} - \varphi^J}{j_{L,k+1} + j_{L,k} - \varphi^J}, \\ \varepsilon_{R,k}^J &= -\mathcal{A}^J \frac{j_{L,k+1} - j_{L,k} - \varphi^J}{j_{L,k+1} + j_{L,k} - \varphi^J}. \end{aligned} \tag{6.6}$$

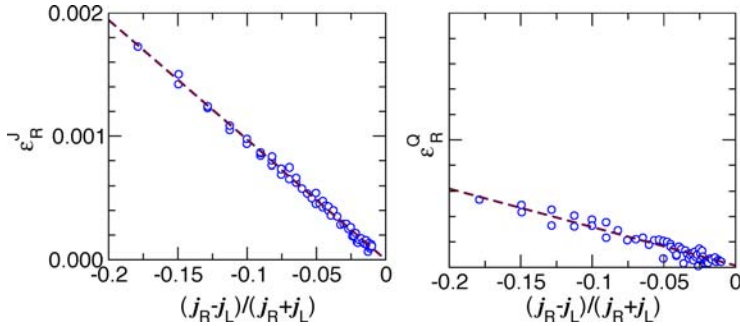


Fig. 6. Dependence of the reflection probabilities $\varepsilon_R^J = \alpha_R^J - \alpha_G^J$ and $\varepsilon_R^Q = \alpha_R^Q - \alpha_G^Q$ on the gradients of the local fields for a chain of 20 RDM cells with $\gamma = 0.08$. The left reflections are $\varepsilon_L^J = -\varepsilon_R^J$ and $\varepsilon_L^Q = -\varepsilon_R^Q$. The external gradients were fixed to $j_> = 1$, $j_< = 6$, and $q_> = q_< = 1500$. The values for the α_G 's have been taken from the data of Fig. 3. The dashed lines correspond to linear fits. (Color online).

Finally, inserting (6.6) into (6.4) we obtain a closed equation for j_L with only one system dependent free parameter, \mathcal{A}^J . In the scaling limit one finds the following nonlinear differential equation for the injection rates:

$$j_L'(\xi) = -\frac{\alpha_G^J(n(\xi)) - \mathcal{A}^J}{1 - \alpha_G^J(n(\xi)) + \mathcal{A}^J} (N\varphi^J) + \mathcal{O}\left(\frac{1}{N}\right). \tag{6.7}$$

The same equations hold for the “R” versions but with different boundary conditions.

Note that φ^J is the current of a chain of length N , and hence is asymptotically equal to Φ^J/N . Using (6.7), Φ^J can be determined by the boundary conditions as

$$\Phi^J = \frac{j_> - j_<}{\int_0^1 W^J(\xi) d\xi},$$

where $W^J(\xi)$ is the coefficient of φ^J in Eq. (6.7).

As discussed in Sec. 5 (see *e.g.*, Fig. 3), we have found that at sufficiently low or high densities, the α depends little on the local fields, taking practically a constant value. Therefore, if the external gradient imposed by the injection of the reservoirs into the system is such that the density in all the cells of the chain is either low ($n \lesssim 0.3$) or high ($n \gtrsim 10$) then the $\alpha_G(n(\xi))$ can be taken as constant along the chain. In this situation Eq. (6.7) gives a linear profile for the injection rate, $\partial_\xi j_L(\xi) = \text{const}$. In particular, in the high density regime, linear profiles will be obtained even when the gradients are very large and the system is far from equilibrium.

For intermediate densities, it follows from (3.4) that α_G is a function of

$$\sqrt{\frac{(j_L + j_R)^3}{q_L + q_R}},$$

which to lowest order in $1/N$ is

$$n(\xi) \propto \sqrt{\frac{j_L^3(\xi)}{q_L(\xi)}}. \tag{6.8}$$

Therefore, in the intermediate density regime, where we have found that $\alpha_G(n)$ is a linear function of n , Eq. (6.7) leads to a system of two explicit coupled differential equations for j and q , which can be solved.

The consistency of our approximations was checked for the RDM model by combining the measurements of all the quantities appearing in Eq. (6.7). The results for the discrete version of this equation are summarized in Fig. 7, which shows good agreement with the theory. These measurements also show, that while correlations are to be expected for high gradients,^(5,10) they do not seem to affect the validity of our approximations.

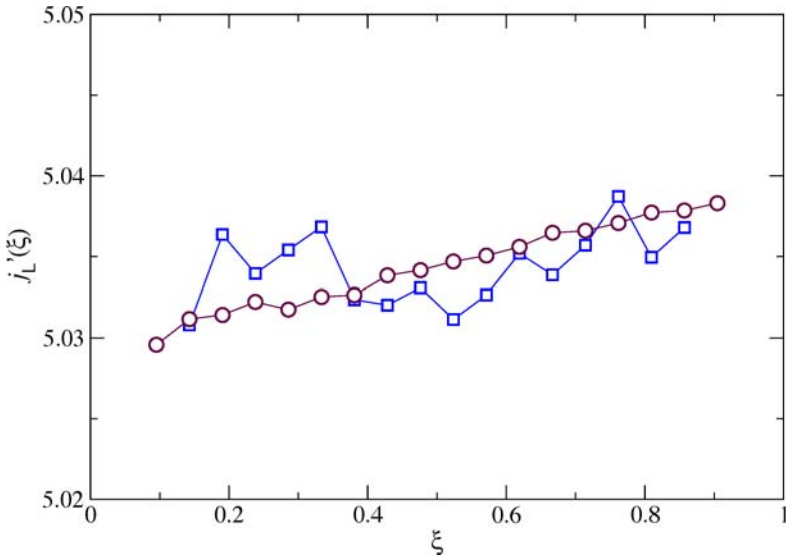


Fig. 7. Numerical verification of Eq. (6.7), for j'_L , for systems of size $N = 20$. The external parameters are those of Fig. 6. The circles correspond to the r.h.s. of (6.7) as explained in the text, while the squares correspond to $(j_{L,k+1} - j_{L,k})(N + 1)$ —measured at $\xi = k/(N + 1)$ —which is an approximation to $j'_L(\xi)$. (Color online).

The external parameters used are those of Fig. 6, which guarantee that all densities along the chain lie in the domain of linear dependence shown in Fig. 3, *i.e.*, between 0.3 and 10. The data in Fig. 7 were obtained as follows: The derivatives j'_L were approximated with centered differences along the profiles. The α_G was read off the linear fit of Fig. 3. The flux φ is directly read off the simulations, while the \mathcal{A} coefficients are obtained from the slope in Fig. 6.

7. CONCLUSIONS

Guided by a stochastic description, we developed a phenomenological description of heat and matter transport for a family of Hamiltonian models of many interacting particles. The description is based on a careful analysis of the way in which particles and energy enter and leave the individual cells.

A stochastic model for a Hamiltonian system must include an appropriate treatment of the memory effects that arise due to the deterministic character of the dynamics. This approach would be cumbersome. Instead, we followed a different approach that, inspired by an approximated stochastic model, is based on the phenomenology of reflection probabilities of particles and of energy in terms of the local fields and the local gradients.

We have expressed a set of balance equations, accounting for particle and energy conservation in the steady state in terms of the reflection probabilities. After specifying a phenomenological law for these probabilities we obtain closed expressions for the local fields and show that they capture the essential features of the microscopic dynamics including memory effects inherent to any Hamiltonian deterministic system.

A useful observation was to identify two contributions to the memory effects: one of geometrical and another of dynamical origin. Close to equilibrium the geometric component dominates and the corresponding correction preserves the “gradient” character of the system. The theory remarkably predicts the transport properties of our class of Hamiltonian models, namely the fluxes of heat and matter and the steady state energy and density profiles.

Far from equilibrium, the dynamical effects strongly depend on the local gradients of the thermodynamical fields and thus, on the particular interaction between particles and energy tanks. Finally, we have shown that in the continuum limit the system is no longer of “gradient” type and the energy and particle currents are not proportional to the external gradients. We have obtained the lowest-order deviation from the theory in Ref. 1. However, we have found that the gradient type condition is restored in the limit of very high or very low densities.

Given that the dynamical memory effects depend on the particular nature of the interaction, our explicit solution (*e.g.*, the particular case of (6.7)), cannot be applied to a general context. However, the program outlined and the variables used

in our derivation are valid and appropriate for the family of models that we have considered.

ACKNOWLEDGMENTS

We thank G. Jona-Lasinio for enlightening discussions and the anonymous referees for useful questions and remarks concerning an earlier version of this paper. This work was partially supported by the Fonds National Suisse.

REFERENCES

1. J.-P. Eckmann and L.S. Young, Nonequilibrium energy profiles for a class of 1-d models, *Commun. Math. Phys.* **262**:237–267 (2006).
2. C. Mejía-Monasterio, H. Larralde and F. Leyvraz, Coupled normal heat and matter transport in a simple model system, *Phys. Rev. Lett.* **86**:5417–5420 (2001).
3. H. Larralde, F. Leyvraz and C. Mejía-Monasterio, Transport properties of a modified Lorentz gas, *J. Stat. Phys.* **113**:197–231 (2003).
4. E. G. D. Cohen and L. Rondoni, On some derivations of irreversible thermodynamics from dynamical systems theory, *Physica D* **168**:341–355 (2002).
5. H. Spohn, *Large Scale Dynamics of Interacting Particles* Text and monographs in Physics (Heidelberg: Springer-Verlag, 1991).
6. H. van Beijeren, Transport properties of stochastic Lorentz models, *Rev. Mod. Phys.* **54**: 195–234 (1982).
7. F. Bonetto, J. L. Lebowitz and L. Rey-Bellet, Fourier's law: A challenge for theorists. In: *Mathematical Physics 2000* (London: Imp. Coll. Press, 2000) pp. 128–150.
8. S. Lepri, R. Livi and A. Politi, Thermal conduction in classical low-dimensional lattices, *Phys. Rep.* **377**:1–80 (2003).
9. A. Dhar and D. Dhar, Absence of local thermal equilibrium in two simple models of heat conduction, *Phys. Rev. Lett.* **82**:480 (1998).
10. G. Nicolis and M. M. Mansour, Onset of spatial correlations in nonequilibrium systems: A master-equation description, *Phys. Rev. A* **29**:2845–2853 (1984).
11. K. Uchiyama, Equilibrium fluctuations for zero-range-exclusion processes. *J. Stat. Phys.* **115**:1423–1460 (2004).